parison of results of MCT calculations and 3D-DFT convolution shows that the latter method is a precise tool for determining absorbed dose and dose-rate profiles for any given spatial activity distribution. Thus, the 3D-DFT convolution method can be used on a patient-specific basis to determine the dosimetry of tumors, organs and user-defined VOIs.

ACKNOWLEDGMENTS

This work was supported in part by Department of Energy grant DE-FG02-91ER61195 and National Cancer Institute grant U01 CA58272-03.

REFERENCES

1. Leichner PK, Koral KF, Jaszczak RJ, Green AJ, Chen GTY, Roeske JC. An overview of imaging techniques and physical aspects of treatment planning in radioimmunotherapy. *Med Phys* 1993;20:569–577.
2. Johnson TK. MABDOS: A generalized program for internal radionuclide dosimetry. *Comput Meth Progr Biomed* 1988;27:159–167.
3. Meredith RF, Johnson TK, Plott G, et al. Dosimetry of solid tumors. *Med Phys* 1993;20:583–592.
4. Berger MJ. Beta-ray dosimetry calculations with the use of point kernels. In: Cloutier RJ, Edwards CL, Snyder WS, eds. *Medical radionuclides: radiation dose and effects*. Oak Ridge, TN: AEC Symposium Series No. 20, CONF 691212; 1970;36–42.
5. Sgouros G, Barest G, Tekumthala J, et al. Treatment planning for internal radionuclide therapy: three-dimensional dosimetry for nonuniformly distributed radionuclides. *J Nucl Med* 1990;31:1884–1891.
6. Leichner PK. A unified approach to photon and beta particle dosimetry. *J Nucl Med* 1994;35:1721–1729.
7. Giap HB, Macey DJ, Podoloff DA. Development of a SPECT-based treatment planning system for radioimmunotherapy. *J Nucl Med* 1995;36:1885–1894.
8. Hawkins WG, Leichner PK, Yang N-C. The circular harmonic transform for SPECT and boundary conditions on the Fourier transform of the sinogram. *IEEE Trans Med Imaging* 1988;7:135–148.
9. Leichner PK, Hawkins WG, Yang N-C. Quantitative SPECT in radioimmunotherapy [Abstract]. *Antibod Immunoconj Radiopharm* 1990;4:25.
10. Hawkins WG, Yang N-C, Leichner PK. Validation of the CHT algorithm for quantitative SPECT. *J Nucl Med* 1991;32:141–150.
11. Leichner PK, Vriesendorp HM, Hawkins WG, et al. Quantitative SPECT for ^{111}In-labeled antibodies in the livers of beagle dogs. *J Nucl Med* 1991;32:1442–1444.
12. Nelson WR, Hirayama H, Rogers DWO. The EGS4 code system. Stanford Linear Accelerator Center. Report 265; 1985.
13. Bielajew AF, Rogers DWO. PRESTA, the parameter reduced electron-step size transport algorithm for electron Monte Carlo transport. National Research Council of Canada Pub. PIRS-0042; 1991.
14. Burrows TW. The program RADLST. Information Analysis Center Report. Report. BNL-NCS-52142. Brookhaven National Laboratory; Upton, NY: 1988.
15. Proceedings at the 12th annual international conference on the IEEE. *Eng Med Biol Soc* 1990;376–378.
16. Metz CE, Pax X. A unified analysis of exact methods of inventing the two-dimensional exponential radon transform with implications for noise control in SPECT. *IEEE Trans Med Imag* 1995;14:643–658.
17. Hawkins WG, Leichner PK. An intrinsic 3D Wiener filter for the deconvolution of spatially varying collimator blur. *Proceedings of the First IEEE International Conference on Image Processing* 1994;2:163–168.
18. Burrus CS and Parks TW. The discrete Fourier transform. In: Burrus CS, Parks TW, eds. *DFT/FFT and convolution algorithms*, 1st ed. New York: John Wiley & Sons; 1985:21–80.
19. International Commission on Radiation Units and Measurements. *Tissue substitutes in radiation dosimetry and measurement*. ICRU Report 44. Bethesda: Press; ICRU 1988.
20. Cristy M, Eckerman KF. Specific Absorbed Fractions of Energy at Various Ages from Internal Photon Sources. I. Methods. Report ORNL/TM-8381/V1. Oak Ridge, TN: Oak Ridge National Laboratory; 1987.
21. Snyder WS, Ford MR, Warner GG and Watson SB. "S', absorbed dose per unit cumulated activity for selected radionuclides and organs. *MIRD pamphlet no. 11*. New York: Society of Nuclear Medicine; 1975.
22. Sauer OA. Calculation of dose distribution in the vicinity of high-Z interfaces for photon beams. *Med Phys* 1995;22:1685–1690.

Quantitative Blood Flow Measurement of Skeletal Muscle Using Oxygen-15-Water and PET

Ulla Ruotsalainen, Maria Raitakari, Pirjo Nuutila, Vesa Oikonen, Hannu Sipilä, Mika Teräs, M. Juhani Knuuti, Peter M. Bloomfield and Hidehiro Iida

Turku PET Center and Department of Medicine and Nuclear Medicine, University of Turku, Turku, Finland; MRC, Cyclotron Unit, London, United Kingdom; and Department of Radiology and Nuclear Medicine, Research Institute for Brain and Blood Vessels, Akita, Japan

The aim of the present study was to evaluate quantitation of muscle blood flow using [^{15}O]H_2O and PET. **Methods:** The autoradiographic (ARG) and the steady-state methods using PET were used to measure femoral muscle blood flow. A simulation study was performed to examine the errors due to contamination of radioactivity in the blood content in muscle tissue, statistical noise and delay and the dispersion of the input curve in the ARG method. Five separate paired muscle blood flow examinations were carried out for comparison of the ARG and the steady-state techniques, including measurement of muscle blood volume in each subject. To obtain the normal range for resting muscle blood flow, additional measurements with the ARG method were performed in 16 normal subjects. **Results:** When the integration time in ARG was increased to 200–300 sec, the errors due to arterial blood volume, statistical noise, delay and dispersion of the input curve were significantly reduced. Muscle blood flow values in the ARG (200 sec) and the steady-state studies were in good agreement, and each provided an estimated accuracy of 5%. Resting muscle blood flow averaged 3.12 ± 1.55 ml/min · 100 g muscle (range 1.43–6.72 ml/min · 100 g muscle, n = 18). **Conclusion:** The ARG and the steady-state methods provided consistent blood flow values for skeletal muscle when a long tissue integration time (≥200 sec) was applied in the ARG study. Based on the lower effective radiation dose and the shorter total scan duration, the ARG method is favored over the steady-state method in the measurement of muscle blood flow.

Key Words: PET; muscle blood flow; low flow

J Nucl Med 1997; 38:314-319

Measurement of metabolite exchange across skeletal muscle requires quantitation of blood flow through the muscle bed (*1*). Reduced blood flow has been suggested to be one of the mechanisms leading to insulin resistance in skeletal muscle (*2*). Peripheral flow studies have previously been performed with plethysmography (*3*) or dilution techniques (*2,4*), which give a measure of whole limb blood flow, including blood flow to skin, adipose tissue and bone in addition to muscle flow. Direct quantitation of muscle blood flow has been performed using the ^{133}Xe clearance technique (*5,6*), which has techni-

Received Oct. 26, 1995; revision accepted Apr. 3, 1996.

For correspondence or reprints contact: Ulla Ruotsalainen, MSc, Turku PET Center, Kiinamyllynkatu 4–6, FIN-20520 Turku, Finland.

cal difficulties in repeat flow measurements due to long tracer decay (5.5 days).

PET provides functional blood flow images, where selected tissues can be outlined. PET and $[^{15}O]H_2O$ have previously been used for quantification of regional blood flow in brain (*7,8*) and heart tissues (*9–11*) regions where most of the evaluations and simulations in blood flow methodology have been performed. When compared with the flow range of 20–100 ml/min · 100 g tissue in the brain, resting skeletal muscle blood flow represents a very low flow level (1.0–2.2 ml/min · 100 g) (*5*). The main error source in the low-flow area is the very low tissue uptake of the tracer, which increases the errors due to the contribution of arterial blood volume, statistical noise and delay of the arterial input function. Also, the effect of dispersion correction of the arterial input curve may be different from the high-flow range.

In this study, two well-known methods for measuring of regional blood flow using $[^{15}O]H_2O$ and PET, the autoradiographic (ARG) and the steady-state methods, were applied for quantitation of muscle blood flow. The accuracy and practical procedure of the methods were evaluated in the simulations and in volunteer studies, and the resting muscle blood flow range in normal subjects was determined.

THEORY

Autoradiographic Method

The methods to measure blood flow with $[^{15}O]H_2O$ are based on the principle of inert gas exchange between blood and tissues developed by Kety (*12*). It has been shown (*13*) that kinetics of $[^{15}O]H_2O$ can be modeled mathematically with a single-compartment model. The autoradiographic method (ARG) has been widely used to numerically solve the flow f (ml/min · 100 g) from the following equation:

$$\int_0^T C_t(t)dt = \int_0^T fC_a(t) * \exp\left(-\frac{f}{p}t\right)dt. \qquad \text{Eq. 1}$$

The right side of the equation can be calculated from the measured decay-corrected arterial time-activity curve $C_a(t)$ (radioactivity concentration as a function of time) for different flow levels assuming a constant value for the partition coefficient of water p in muscle. The asterisk denotes the convolution integral. The left side of the equation is the pixel-by-pixel solved integral of the decay-corrected tissue time-activity curve. A table look-up procedure from the left side to the right side gives a rate constant for flow f in the integration time scale T (*14*). The true input function for the tissue element is not exactly known because the measured arterial input curve suffers from external dispersion due to the sampling system, as well as from internal dispersion in the arterial line of the arm. There is also a delay between the measured input curve and the real entrance of the tracer into the tissue. The dispersion of the measured input curve can be described with a first-order exponential function (*13*). The true input function can be solved by deconvolving the measured input curve with the dispersion function. Because there are two sources of dispersion in this case, the tubing and the peripheral artery, this deconvolution process is done twice with two different dispersion time constants. The delay is solved by fitting the input curve, corrected for dispersion, into the measured tissue time-activity curve (*13*).

Steady-State Method

This method for assessing regional blood flow is based on continuous administration of either $[^{15}O]H_2O$ or $[^{15}O]CO_2$. The tissue activity concentration reaches an equilibrium when the constant administration of the activity is in balance with the washout and the physical decay of the tracer in the muscle (*7*). During this condition, blood flow can be solved as:

$$f = \frac{\lambda}{\frac{C_{a\text{-}avg}}{C_{t\text{-}avg}} - \frac{1}{p}}. \qquad \text{Eq. 2}$$

In the equation, λ denotes the physical decay constant of $[^{15}O]$, p is the partition coefficient of water in muscle tissue, and $C_{a\text{-}avg}$ and $C_{t\text{-}avg}$ are the average radioactivity concentrations in blood and tissue, respectively, during the steady-state condition.

MATERIALS AND METHODS

Simulation Studies

Time-Activity Curves. Tissue time-activity curves were generated with the assumed flow value of 4 ml/min · 100 g and 10 ml/min · 100 g and for slow bolus as used in ARG. The partition coefficient of water p was assumed to remain constant in muscle tissue. It was calculated by dividing the fractional water content of muscle (79%, 75.96 ml/100 g) by the fractional water content of blood (80 ml/100 ml), giving the estimation of 0.95 ml/g (*15*). The time-dependent tissue activity curve was calculated as

$$C(t) = fC_a(t) * \exp\left(-\frac{f}{p}t\right) + V_aC_a(t), \qquad \text{Eq. 3}$$

where V_a represents the arterial blood volume component, assumed to be related to the blood content (V_B) in the muscle as $V_a = 0.1 \cdot V_B$ (*16*). With the measured whole-blood volume of 0.03 ml/g in muscle (*17*), the arterial blood volume (V_a) was estimated to be 0.003 ml/g. The equation was solved for the time range from 0 to 360 sec in 1-sec steps. The input curve used in the simulations was a typical measured blood time-activity curve of the volunteers, corrected for dispersion and delay except when the errors caused by these sources were evaluated. In the steady-state method, the tissue radioactivity concentration was calculated according to Equation 2 with the average blood radioactivity concentration in the subjects. The effect of arterial blood volume was included similarly as in ARG method.

Error from Arterial Blood Volume. The error due to varying arterial blood volume in muscle was studied as a function of integration time in ARG for the flow of 4 ml/min · 100 g. In the steady-state simulation study, this error was evaluated as a function of flow.

Error from Dispersion and Delay in ARG. The input curve was corrected for the dispersion effects from the tubing and the radial artery line to get the reference flow value. Thereafter, the dispersion correction was made to the original input curve by varying the dispersion time constant in 1-sec steps. The blood-flow values were calculated with ARG method for various integration times. The effect of delay on the relationship between the input curve and the tissue curve was evaluated similarly by shifting the input curve forward and backward from the original position along the time axis in 5-sec steps.

Error from the Partition Coefficient of Water. The error sensitivity to the assumed partition coefficient of water in muscle was investigated for the ARG and steady-state methods.

Statistical Noise. The pixel-by-pixel noise in the ARG measurement was estimated by calculating the coefficient of variation for flow rates of 4 and 10 ml/min · 100 g. The tissue radioactivity concentration was calculated according to Equation 3 and converted to counts per second with the sensitivity of ECAT 931

scanner (3926 counts/s · MBq) (*18*). This tissue time-activity curve was integrated over various integration times (from 30 to 360 sec), and the pixel-by-pixel deviation was defined as square root of total counts per pixel. This deviation was applied to the ARG look-up table to find the estimated deviation in flow value (*19*).

Subjects and Study Design

Twenty men (age 33.0 ± 8.2 yr, BMI 24.4 ± 3.3 kg/m^2) volunteered in the study. The nature, purpose and potential risks of the study were explained to all subjects before they gave their voluntary informed consent to participate. The study was approved by the Ethical Committee of the Turku University Central Hospital. All studies were performed after an overnight fast. Two catheters were inserted, one in an antecubital vein for infusion of [^{15}O]H_2O and another for blood sampling in the opposite radial artery. Four men participated in the comparative study of the ARG and steady-state methods. Three of these subjects were healthy as jugded by physical examination and routine laboratory tests and were not taking any medication, and one subject received medication for hypertension. Femoral muscle blood flow was measured with the ARG and the steady-state methods in the basal state only (n = 2), in the basal state and during euglycemic hyperinsulinemia (n = 1) and during hyperinsulinemia only (n = 1). Insulin was used in two of the examinations to stimulate muscle blood flow (*2*). Muscle blood volume was measured once in each subject. For determination of the normal flow range, muscle blood flow was measured with the ARG method in the basal state in an additional 16 healthy men.

PET Procedure

Oxygen-15 Products. Oxygen-15 compounds were produced in a low-energy deuteron accelerator Cyclone 3 (IBA, Ion Beam Application Inc., Louvain-la-Neuve, Belgium). [^{15}O]H_2O was produced using dialysis techniques in a continuously working water module (*20*). An online radioactivity recording of infusions was done for each examination with a low voltage ionization chamber (*21*). [^{15}O]O was processed to [^{15}O]CO in a charcoal oven at 950°C.

Image Acquisition. An eight-ring ECAT 931/08-tomograph (Siemens/CTI Corp., Knoxville, TN) was used. The scanner has an axial resolution of 6.7 mm and in-plane resolution of 6.5 mm FWHM (*22*). The subject was positioned in the tomograph with the femoral regions in the gantry. Before emission scan, a transmission scan for the correction of photon attenuation was performed for 15 min with a removable ring source containing ^{68}Ge (total counts 15–30 × 10^6 per plane). All data were corrected for deadtime, decay and measured photon attenuation and reconstructed into a 128 × 128 matrix using Hann filter with the cutoff frequency of 0.5. The observed final in-plane resolution was 8 mm.

Steady-State Flow. Muscle blood flow was measured by infusing [^{15}O]H_2O intravenously at a speed of 185 MBq/min for 25 min. The infused dose was 4500 ± 570 MBq (range 4000–5290 MBq). At 10 min from the beginning of the infusion, when steady state had been reached, a dynamic scan of the femoral region was started for 15 min (15 × 60 sec). Tissue radioactivity was measured continuously throughout the study with an external radiation detector to confirm the steady-state condition. Arterial blood samples were withdrawn every 60 sec and the radioactivity concentration was measured with a well counter. The total counts collected in the femoral region were approximately 1.5 × 10^5 during the 10-min period. The measured activity concentrations in blood and tissue were examined, and the most stable 10-min period was chosen for flow calculations.

Autoradiographic Method. A dynamic 6-min scan was started simultaneously with the 30-sec intravenous infusion. The administered dose in the ARG study was 1730 ± 130 MBq (range 1290–1960 MBq). To obtain the input function, arterial blood was withdrawn with a pump at a speed of 6.0 ml/min from the radial artery, and the radioactivity concentration was measured using a two-channel detector system calibrated to the well counter and the PET scanner. A dispersion time constant of 3 sec was measured with the tubing of the online detector (*13*) when the artery-to-detector separation was 20 cm. The internal dispersion time constant for radial artery was assumed to be 5 sec (*13*). The collected counts per second for the femoral region were approximately 3.5 × 10^5.

Measurement of Muscle Blood Volume. A static scan of the femoral region was performed after 2 min from the end of the 2-min inhalation of [^{15}O]CO (0.14% mixed with room air), as previously described (*17*). During the 4-min scan period, three blood samples were taken and the radioactivity concentration in blood was measured with the well counter. The inhaled dose in the CO examinations was 4780 ± 700 MBq (mean ± s.d., range 4000–5800 MBq). Regional muscle blood volume was calculated under steady-state conditions by dividing the tissue radioactivity concentration by the activity concentration in blood (*17*).

Regions of Interest. Regions of interest (ROIs) were drawn on the anterolateral and posterior muscular areas in the steady-state flow images (*17*). The same ROIs were copied to the ARG and the blood volume images to obtain data from identical regions. The results were averaged values from four adjacent planes.

Statistical Procedures. Student's t-test and linear regression analysis with Pearson's correlation coefficient were applied to the data. All results are expressed as mean ± s.d. (s.d.).

RESULTS

Results of Simulation Studies

The radioactivity concentration in the arterial blood content in muscle tissue led to an overestimation of the integrated tissue counts in both ARG and steady-state methods and consequently to overestimation of flow. In ARG, prolonging the integration time decreased the error significantly (Fig. 1A). In the steady-state method, the relative error from arterial blood contribution in muscle was only a function of blood flow (Fig. 1B). The errors in (correcting the dispersion (Fig. 2B) of the input function) determining the time delay (Fig. 2A) between the input curve and tissue time-activity curve produced a greater error into the resulting blood flow values with a shorter integration time than with a longer time in the ARG method. The error from the partition coefficient of water in muscle was slightly greater in the higher (10 ml/min · 100 g) than lower (4 ml/min · 100 g) flow range and was also more pronounced in the steady-state method than in ARG.

The simulated pixel-by-pixel statistical noise propagation for various flow values is shown in Figure 3 for ARG as a function of integration time. With the flow values of 4–10 ml/min · 100 g, statistical noise was constantly decreasing with increasing integration time.

Human Studies

In the parametric ARG and steady-state flow images, higher flow rates were observed in the great arteries, while flow in skeletal muscle remained low (Fig. 4A, B). Great veins were prominent in the muscle blood volume image (Fig. 4C). Quantitative muscle blood flow rates and muscle blood volumes are shown in Table 1. Regional muscle flow values in the steady-state and ARG measurements with a 200-sec integration time were in good correlation ($r = 0.84$, $p < 0.01$, Fig. 5) and did not differ significantly. The flow in the anterolateral and posterior muscle areas were significantly different ($p < 0.05$, Table 1). In the ARG method, shorter integration times (40 sec

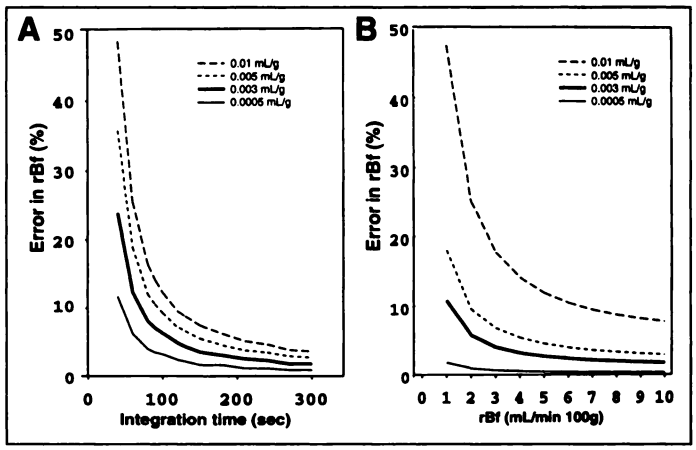

FIGURE 1. Simulations showing systematic error from radioactivity in arterial blood with the various estimated blood volumes. (A) ARG shown as a function of integration time and (B) the steady-state method as a function of flow.

and 90 sec) resulted in significantly higher muscle blood flow values as compared with the 200-sec integration time (Table 2). The pixel-by-pixel s.d. in the flow images approached the s.d. of the steady-state flow image, when the integration time was extended to 200 sec (Fig. 6). The estimated effective doses with the administered tracers in the present study were 2.1 mSv in the ARG study and 5.4 mSv in the steady-state study (*23*).

When measured with the ARG method in 18 normal subjects, muscle blood flow in the posterior muscle area averaged 3.12 ± 1.55 ml/min · 100 g muscle (range 1.43–6.72 ml/min · 100 g muscle).

DISCUSSION

The ARG and steady-state methods gave consistent results for skeletal muscle blood flow when a long integration time was chosen in ARG. The flow range in the resting femoral muscle measured with ARG in normal subjects, 1.43–6.72 ml/min · 100 g muscle, was of the same order as the flow values determined with other methods in previous studies (*2,3,5*). We recently compared PET and ARG with plethysmography for measurement of limb blood flow and obtained similar flow values (2.8 versus 2.5 ml/min · 100 g) (*24*). The femoral muscle was chosen in this study because relatively large ROIs may be selected, thus maximizing count statistics. Significantly higher flow values were observed in the anterolateral muscle region as compared with the posterior muscle area (Table 1), which might be due to physiological true difference or spillover from the

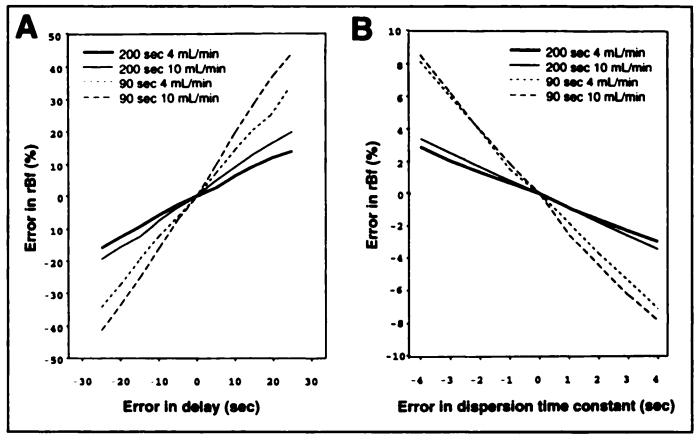

FIGURE 2. Simulation of the error in regional blood flow (rBf) caused by the errors (A) in delay adjustment and (B) in the correction of dispersion in the ARG study.

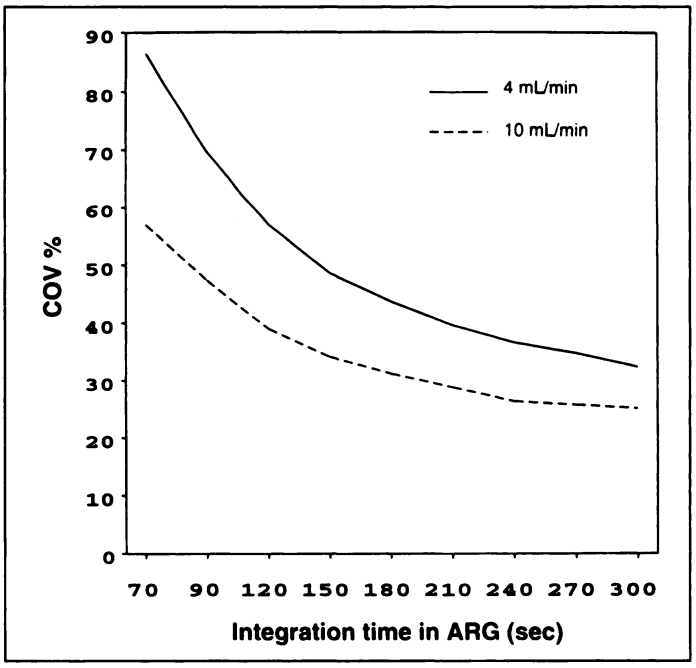

FIGURE 3. Simulated noise propagation as a function of integration time in the ARG study.

blood activity in the femoral artery. The relatively wide range of resting muscle flow is probably caused by the physiological variability among healthy subjects and may also reflect the level of physical fitness (*25*). Despite the large flow range, we could detect significant changes in flow during pharmacological stimulations (*24*).

ARG

The ARG method is rather rapid, requiring a study period of only 3–6 min. However, it needs a continuous arterial input curve for the entire data acquisition period. In the simulation study for low flow (Fig. 2A), a 10-sec delay of the input curve introduced an error of 20% in the calculated blood flow with a 90-sec integration time. When the integration time was extended to 200 sec, the error was reduced to 10%. The error from dispersion was also shown to decrease with increasing integration times. For example, the interindividual variation (±2 sec) in the internal dispersion time constant (*13*) caused an error of 30% into the calculated blood flow with a 40-sec integration time. The error decreased to 2% with a 200-sec integration time in the simulations.

Despite the small volume of arterial blood in muscle tissue, its activity concentration interfered with the shape of the whole tissue time-activity curve in ARG, particularly at the beginning because of the extremely low radioactivity concentration in the tissue. This caused an error in calculated flow which decreased with increasing integration times, approaching a constant level, which depended on the estimated blood volume (Fig. 1A). The estimation of the transit time between the arterial sampling site and the femoral muscle was also affected by the arterial

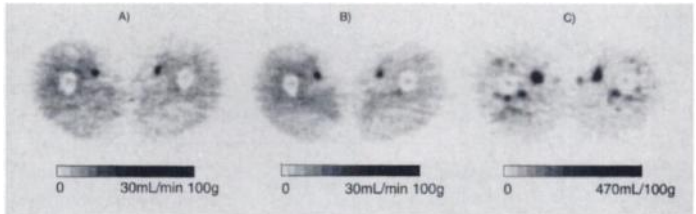

FIGURE 4. Pixel-by-pixel flow images for (A) ARG and (B) steady-state methods and (C) blood volume image in the same subject.

TABLE 1
Results from Blood Flow and Blood Volume Measurements

Study no.	Area	Steady-state flow (10 min) (ml/min · 100 g muscle)	ARG flow (200 sec) (ml/min · 100 g muscle)	Blood volume (ml/100 g muscle)
1	Post	3.38	2.45	—
	Ant	5.66	4.43	—
2	Post	3.92	4.13	4.13
	Ant	7.68	7.80	5.04
3	Post	3.06	3.66	3.65
	Ant	5.22	4.98	5.06
4*	Post	3.64	5.02	2.38
	Ant	4.55	5.49	3.71
5*	Post	3.78	4.27	3.18
	Ant	5.88	7.09	4.94
Mean ± s.d.	Post	3.56 ± 0.31	3.91 ± 0.85	3.33 ± 0.65
	Ant	5.80 ± 1.04	5.96 ± 1.28	4.69 ± 0.57

*The study was performed during insulin stimulation.
Post = posterior muscle area; Ant = anterolateral muscle area.

radioactivity contribution, the time shift being approximately 3 sec with the estimated arterial blood volume of 0.003 ml/g. This error due to arterial radioactivity was reduced with a long integration time.

The calculated flow values of the subjects decreased significantly as the integration time in ARG was increased from 40 sec to 200 sec (Table 2). This may be explained by the effects of arterial blood volume or imperfect correction for delay or the dispersion of the arterial input curve, which, as has been shown, are more critical error sources with a short rather than long integration time. A long integration time was also optimal statistically. However, the blood flow-to-PET counts linearity still remained with long scan durations. All total, with an integration time longer than 200 sec and with an input curve corrected for delay and dispersion, an accuracy rate of about 5% can be achieved (Fig. 2A, B).

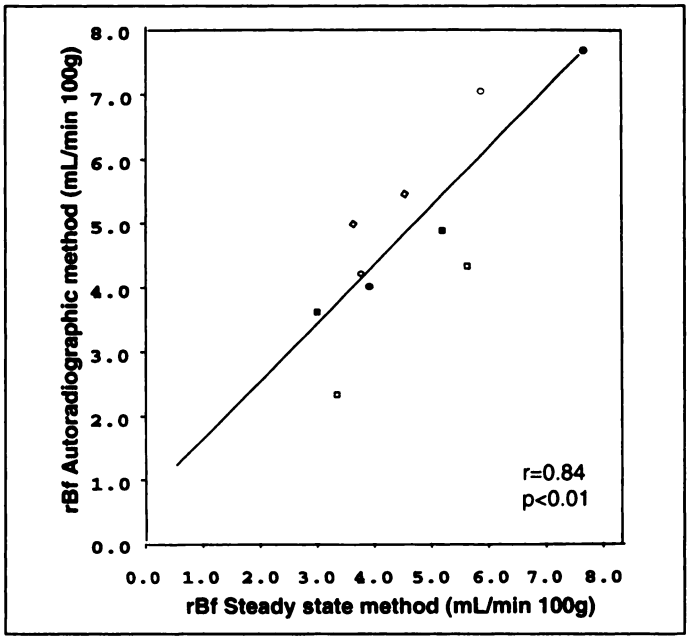

FIGURE 5. Correlation between the flow values determined with the steady-state and ARG methods: y = 0.92 (±0.21)x + 0.63(±1.04) (parameter estimate ± s.e.); s.e.e. = 0.92 ml/min · 100 g. Two ROIs have been outlined for each subject, anterolateral (high-flow) and posterior (low-flow) regions. Each subject has individual symbols for flow values.

TABLE 2
Muscle Blood Flow Values (ml/min · 100 g) with Various Integration Times (Posterior Area)

Study no.	Time (sec) 40	90	200	250
1	3.13	2.84	2.45	2.36
2	4.51	4.38	4.13	3.96
3	4.19	4.10	3.66	3.72
4	6.04	6.07	5.02	4.77
5	6.16	5.15	4.27	3.98
Mean ± s.d.	4.81 ± 1.05*	4.51 ± 0.98*	3.91 ± 0.78	3.76 ± 0.72

*Differs significantly from the values obtained with a 200 sec integration time ($p < 0.05$).

Steady-State Method

In the steady-state method, there are no problems associated with the corrections of the input curve. The contribution of the arterial blood volume in the tissue caused an overestimation of flow, which decreased by increasing flow levels. In the flow range of 2–10 ml/min · 100 g, the error was less than 5%, with an arterial blood volume of 0.003 ml/g (Fig. 1B). In addition to the constant administration of tracer activity, a constant physiological condition is also required throughout the study period greater than 20 min (the time frame used in this study), including the buildup phase and data acquisition (*26*). This may be difficult in typical human studies, especially with repeat examinations. This demand is less limiting in the ARG technique because of the short data acquisition time needed for the measurement.

CONCLUSION

As in brain blood flow studies, the steady-state and the ARG methods using $[^{15}O]H_2O$ and PET gave accurate blood flow values in the low-flow range of muscle tissue when a long integration time was chosen in ARG. Because of the shorter scan duration and lower effective dose to the patient, the ARG method may be more practical, particularly when repeated flow

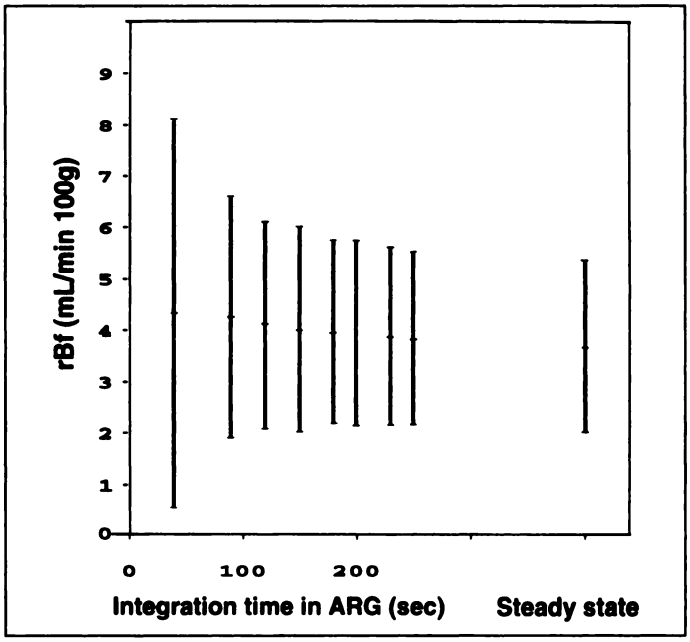

FIGURE 6. Noise propagation (pixel-by-pixel s.d. in the flow image) in the ARG method, using different integration times, and in the steady-state method with a 10-min acquisition time.

measurements are to be performed and provides a useful research tool for the study of muscle metabolism.

ACKNOWLEDGMENTS

This work was supported by grants from the Finnish Culture Foundation (UR), the Sigrid Juselius Foundation (HI and UR) and the Research and Science Foundation of Farmos (MR). We thank the personnel of the Turku PET Center for their cooperation and Kai Niemi for computer programming assistance.

REFERENCES

1. Elia M. The inter-organ flux of substrates in fed and fasted man, as indicated by arterio-venous balance studies. *Nutr Res Rev* 1991;4:3–31.
2. Laakso M, Edelman SV, Brechtel G, Baron AD. Decreased effect of insulin to stimulate skeletal muscle blood flow in obese man. *J Clin Invest* 1990;85:1844–1852.
3. Jackson RA, Peters N, Advani U. Forearm glucose uptake during the oral glucose tolerance test in normal subject. *Diabetes* 1973;22:442–458.
4. Rabinowitz D, Zierler KL. Forearm metabolism in obesity and its response to intra-arterial insulin. Characterization of insulin resistance and evidence for hyperinsulinism. *J Clin Invest* 1962;41:2173–2181.
5. Elia M, Kurpad A. What is the blood flow to resting human muscle? *Clin Sci* 1993;84:559–563.
6. Lassen NA, Lindberg J, Munck O. Measurement of blood flow through skeletal muscle by intramuscular injection of xenon-133. *Lancet* 1964;i:686–689.
7. Frackowiak RSJ, Lenzi G-L, Jones T, Heather JD. Quantitative measurement of regional cerebral blood flow and oxygen metabolism in man using ^{15}O and positron emission tomography: theory, procedure and normal values. *J Comput Assist Tomogr* 1980;4:727–736.
8. Huang S-C, Carson RE, Hoffman EJ, et al. Quantitative measurement of local cerebral blood flow in humans by positron computed tomography and ^{15}O-water. *J Cereb Blood Flow Metab* 1983;3:141–153.
9. Iida H, Kanno I, Takahashi A, et al. Measurement of absolute myocardial blood flow with $H_2{}^{15}O$ and dynamic positron emission tomography. Strategy for quantification in relation to the partial-volume effect. *Circulation* 1988;78:104–115.
10. Bergmann SR, Herrero P, Markham J, Weinheimer CJ, Walsh MN. Noninvasive quantitation of myocardial blood flow in human subjects with oxygen-15-labeled water and positron emission tomography. *J Am Coll Cardiol* 1989;14:639–652.
11. Iida H, Takahashi A, Tamura Y, Ono Y, Lammertsma A. Myocardial blood flow: Comparison of oxygen-15-water bolus injection, slow infusion and oxygen-15-carbon dioxide slow inhalation. *J Nucl Med* 1995;36:78–85.
12. Kety SS, Schmidt CF. The determination of cerebral blood flow in man by the use of nitrous oxide in low concentrations. *Am J Physiol* 1945;143:53–66.
13. Iida H, Kanno I, Miura S, Murakami M, Kazuhiro T, Uemura K. Error analysis of a quantitative cerebral blood flow measurement using $H_2{}^{15}O$ autoradiography and positron emission tomography with respect to the dispersion of the input function. *J Cereb Blood Flow Metab* 1986;6:536–545.
14. Howard BE, Ginsberg MD, Hassel WR, Lockwood AH, Freed P. On the uniqueness of cerebral blood flow measured by the in vivo autoradiographic strategy and positron emission tomography. *J Cereb Blood Flow Metab* 1983;2:99–108.
15. Snyder WS, Cook MJ, Nasset ES, Karhausen LR, Howells GP, Tipton IH, eds. In: *Report of the task group on reference man*, 1st ed. London: Pergamon Press; 1975.
16. Berne RM, Levy MN, eds. In: *Physiology*, 2nd ed. St. Louis: CV Mosby; 1988.
17. Raitakari M, Knuuti MJ, Ruotsalainen U, et al. Insulin increases blood volume in human skeletal muscle. *Am J Physiol* 1995;269:E1000–E1005.
18. Bailey DL, Jones T, Spinks TJ. A method for measuring the absolute sensitivity of positron emission tomographic scanners. *Eur J Nucl Med* 1991;18:374–379.
19. Iida H, Kanno I, Miura S. Rapid measurement of cerebral blood flow with positron emission tomography. In: *Exploring brain functional anatomy with positron tomography*. Chichester: Wiley; 1991:23–42.
20. Crouzel C, Clark J, Brihaye C, et al. Radiochemistry automation for PET. In: Stocklin G, Pike V, eds. *Radiopharmaceuticals for positron emission tomography*. Dordrecht, Netherlands: Kluwer Academic Publishers; 1993: 54–90.
21. Sipilä HT, Heselius S-J, Saarni HK, Ahlfors T. A compact low-voltage ionization chamber for monitoring positron- and photon-emitters in flowing gases. *Nucl Ins Meth Phys Res* 1985;A238:542–545.
22. Spinks TJ, Jones T, Gilardi MC, Heather JD. Physical performance of the latest generation of commercial positron scanner. *IEEE Trans Nucl Sci* 1988;35:721–725.
23. Smith T, Tong C, Lammertsma AA, et al. Dosimetry of intravenously administered oxygen-15-labeled water in man: a model based on experimental human data from 21 subjects. *Eur J Nucl Med* 1994;21:1126–1134.
24. Nuutila P, Raitakari M, Laine H, et al. Role of blood flow in regulating insulin-stimulated glucose uptake in humans. Studies using bradykinin, [^{15}O]water and [^{18}F]fluorodeoxyglucose and PET. *J Clin Invest* 1996;97:1741–1747.
25. Ebeling P, Bourey R, Koranyi L, et al. Mechanism of enhanced insulin sensitivity in athletes. *J Clin Invest* 1993;92:1623–1631.
26. Meyer E, Yamamoto YL. The requirement for constant arterial radioactivity in the $C^{15}O_2$ steady-state blood-flow model. *J Nucl Med* 1984;25:455–460.

Clinical Fusion of Three-Dimensional Images Using Bremsstrahlung SPECT and CT

E. Ishmael Parsai, Komanduri M. Ayyangar, Ralph R. Dobelbower and Jeffry A. Siegel

Department of Radiation Therapy, Medical College of Ohio, Toledo, Ohio; and Department of Radiation Oncology, Cooper Hospital/University Medical Center, Camden, New Jersey

Infusional brachytherapy for treatment of neoplasms, with colloidal ^{32}P has been used to treat various tumors in the pancreas, liver, brain, lung, and head and neck. In performing such treatments, anatomical verification of the location of the administered ^{32}P from the image obtained by Bremsstrahlung SPECT alone is not possible due to the lack of internal landmarks, since the radionuclide is distributed only in the tumor and does not usually accumulate in the normal organs. The purpose of this study was to provide a practical three-dimensional approach for image fusion between Bremsstrahlung SPECT and CT. **Methods:** The tumors in four cancer patients were injected directly with ^{32}P under CT guidance. A Bremsstrahlung SPECT study using ^{99m}Tc backscatter sources to obtain the body contour was then performed. SPECT images were used to generate the skin contours using a threshold detection method. A three-dimensional surface was generated from these contours using a tiling program and fused with a corresponding CT surface generated from a CT scan in the same patient through an iterative surface-fitting algorithm. The three-dimensional surface of the region of high-activity, corresponding to the infused tumor, was then generated using the Bremsstrahlung SPECT data by mapping the iso-count surfaces through a computer program. The three-dimensional image of the organ then was fused with the registered CT-SPECT datasets. **Results:** The accuracy of fit measured as the mean distance between the SPECT and CT surfaces was in the range of 3–4 mm. **Conclusion:** The anatomical co-registration of Bremsstrahlung SPECT with CT images using the outer surface-fitting algorithm is a reliable tool. This correlation permits direct anatomic confirmation of the region of the ^{32}P activity distribution with the anatomic site selected for injection.

Key Words: Bremsstrahlung; SPECT; phosphorus-32; image fusion; radionuclide therapy

J Nucl Med 1997; 38:319–324

SPECT and CT are well-established diagnostic imaging modalities. These modalities provide complementary information, i.e., SPECT provides functional information whereas CT mainly demonstrates morphology. The fusion of SPECT and CT can increase the information provided by either modality

Received Sept. 20, 1995; revision accepted Mar. 6, 1996.

For correspondence or reprints contact: Komanduri M. Ayyangar, PhD, Professor and Chief of Physics, Medical College of Ohio, Department of Radiation Therapy 3000 Arlington Ave., P.O. Box 10008, Toledo, OH 43699-0008.